International Journal of Rotating Machinery 2005:3, 202–210

Investigation of the Optimum Clocking Position in a Two-Stage Axial Turbine

Dieter Bohn
Institute of Steam and Gas Turbines, Aachen University, Templergraben 55, 52056 Aachen, Germany
Email: post-bohn@idg.rwth-aachen.de

Sabine Ausmeier
Institute of Steam and Gas Turbines, Aachen University, Templergraben 55, 52056 Aachen, Germany

Jing Ren
Institute of Steam and Gas Turbines, Aachen University, Templergraben 55, 52056 Aachen, Germany
Email: jing@idg.rwth-aachen.de

Received 4 March 2005

A frozen rotor approach in a steady calculation and a sliding mesh approach in an unsteady simulation are performed in a stator clocking investigation. The clocking is executed on the second stator in a two-stage axial turbine over several circumferential positions. Flow field distributions as well as the estimated performances from two approaches are compared with each other. The optimum clocking positions are predicted based on the estimated efficiency from the two approaches. The consistence of the optimum clocking positions is discussed in the paper. The availability and the limit of the frozen rotor approach in predicting the optimum clocking position is analyzed. It is concluded that the frozen rotor approach is available to search the optimum clocking position in the preliminary design period, although it misses some features of the unsteady flow field in the multistage turbines.

Keywords and phrases: clocking, unsteady, turbine.

1. INTRODUCTION

Recently great attention has been paid to airfoil clocking in the multistage turbomachinery. Such a technique operates on the relative circumferential positions of fixed and rotating blade rows in consecutive stages and aims at performance improvement. The clocking affects the interaction of the wakes and unsteady pressure field from the upstream airfoils with the downstream airfoils. The strength of these interactions can affect both performance and durability of the turbines.

Both experimental and numerical investigations have shown how the time-averaged turbomachinery efficiency varies periodically with stator and rotor clocking positions (Eulitz et al. [1], Reinmoeller et al. [2]). The experimental results reported by Huber et al. [3] for a two-stage HP turbine showed a 0.8% efficiency variation due to clocking of the second-stage stator. A 2D numerical analysis at midspan performed by Griffin et al. [4] for the same turbine correctly predicted the optimum clocking positions but the estimated efficiency variation was only 0.5%. A lot of investigations have proved that the highest efficiencies occurred when the first-stage stator wake impinged on the second-stage stators while the lowest were observed when the first-stage stators wake convected through the mid-passage region between the second-stage stator airfoils (Arnone et al. [5], Dorney et al. [6, 7]). Cizmas and Dorney [8] extended this conclusion to rotor clocking and 2D multistage clocking. They investigated the effects of full clocking (i.e., simultaneously clocking stator and rotor rows) in a three-stage steam turbine. They found that the clocking of the second stage gives larger efficiency variations than the clocking of the third stage. Meanwhile, the benefit of rotor clocking was almost twice that of stator clocking. Bohn et al. [9] investigated a stator clocking in a 3D multistage turbine. They suggest a similar principle between the wake trajectories on the midspan and the total-to-total turbine efficiency.

While previous efforts have provided considerable insight into the physical mechanisms associated with airfoil

clocking, less attention has been paid to the capability of different numerical algorithms in the clocking investigations. Certainly, the CFD simulation of real turbomachinery flows can be realized using time-dependent numerical methods. Although enormous computer resources are needed for this modeling, it simulates real flow physics best of all. Steady numerical approaches approximate the real flow in turbines, as they neglect some effects of real physics. Nevertheless the steady models are quite popular in industrial use, mainly due to relative short time and less memory usage.

In this paper, a stator clocking in a two-stage axial turbine is investigated by an unsteady and a steady calculation. The purpose of the current work is to investigate the capability and the limit of the steady algorithm in predicting the optimum clocking position.

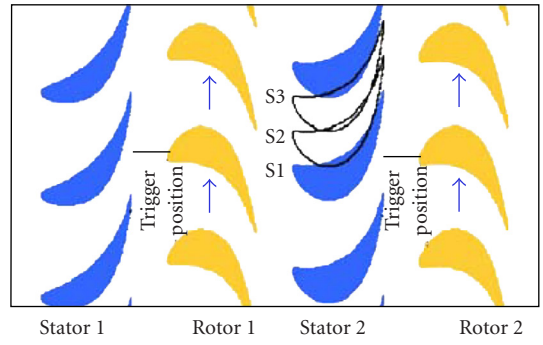

Figure 1: Stage configuration on midspan.

2. NUMERICAL ALGORITHM

Real flow in gas turbines is quite complex, being viscous, unsteady, and three-dimensional. The CFD programs offer different approaches to investigate such a flow field numerically, all of them using multiple reference frames:

(i) the mixing plane model,
(ii) the frozen rotor model,
(iii) the sliding mesh model.

The three approaches above differ in the way that the interface between moving and nonmoving cell zones is treated. In the mixing plane approach, for each fluid zone a steady state solution is calculated. The two adjacent frames are coupled by exchange of flow field variables at the interface. Flow field data are averaged circumferentially for both frames at the interface and then passed to the adjacent zone as boundary conditions. This spatially averaging at the interface removes any unsteadiness that would arise due to variations in the zone-to-zone flow field (e.g., wakes, shock waves, separated flow). The advantage of this approach compared to the frozen rotor model is the less need for computational resources, since due to circumferentially averaging it is sufficient to model only one passage between two adjacent vanes/blades in each rotor/stator.

For the frozen rotor model, the coupling between the cell zones is done by maintenance of absolute velocity in the global coordinate, that is, the velocities are just switched between relative and absolute frames. Thus, one obtains a "snapshot" of the flow field at one fixed rotor position. Wakes between different cell zones are considered in some degree. Therefore, the frozen rotor approach is chosen in the steady investigation in the presented work.

Both the frozen rotor and the mixing plane model assume that the flow field is steady, with the rotor/stator effects being accounted for by approximate means. On the other hand, the sliding mesh model assumes that the flow field is unsteady, and hence models the interaction with complete fidelity. Most often, the unsteady solution that is sought in a sliding mesh simulation is time periodic. Note that since the sliding mesh model requires an unsteady numerical solution, it is computationally more demanding than the frozen rotor and mixing plane approaches.

While the frozen rotor approach is chosen in the steady computations, the sliding mesh approach is used in the unsteady calculations. By comparing the steady results and the unsteady one, the ability and limits of the frozen rotor approach in predicting the optimum clocking positions in multistage turbomachinery are investigated.

3. THE TURBINE STAGES

3.1. Geometry

The investigated turbine cascade is composed of two stages of an axial turbine. Each stator or rotor contains 48 vanes or blades. Figure 1 shows the airfoil cascades on midspan. The trigger position of the rotors is marked by a line which represents the relative position of the rotors to the stators at time $t = 0$.

3.2. Clocking series

The second stator is clocked in steps of 2.5° in a range of one stator pitch to receive 3 stator-stator clocking positions. They are indicated in Figure 1 as clocking position S1, S2, S3, which are corresponding to 0°, 2.5°, 5.0°, respectively.

In the steady calculations, six relative stator-rotor positions passing one rotor pitch are defined. Starting from the rotor's trigger positions indicated in Figure 1, the stator-rotor relative positions are named as R1, R2, R3, R4, R5, and R6 consequently. They are correspondent with 0°, 1.25°, 2.5°, 3.75°, 5.0°, 6.25°, respectively. Therefore, there are $3 \times 6 = 18$ configurations altogether, as each clocking position contains six stator-rotor positions. The frozen rotor approach is applied in each configuration.

For the unsteady calculation, the rotors start from their trigger positions while time t equals 0. In order to compare the unsteady results with the steady one lately, six dimensionless times t/T are chosen in the unsteady calculations. Here, T is one blade-passing period. The corresponding relationship between the dimensionless times t/T and the stator-rotor positions is shown in Table 1.

Table 1: Corresponding relationship between stator-rotor relative position and dimensionless time t/T.

Stator-rotor relative position in steady calculation		Dimensionless time t/T in unsteady calculation
R1 (0.00°)	⟶	0
R2 (1.25°)	⟶	1 / 6
R3 (2.50°)	⟶	1 / 3
R4 (3.75°)	⟶	1 / 2
R5 (5.00°)	⟶	2 / 3
R6 (6.25°)	⟶	5 / 6

Table 2: Boundary conditions.

Inlet total pressure ($\times 10^5$Pa)	3.24
Inlet total temperature (K)	353.80
Exit static pressure ($\times 10^5$Pa)	2.31
Absolute inlet angle (°)	0.00
Rotor speed (1/s)	79.70

3.3. Boundary conditions

The boundary conditions of the cascades described above are given in the Table 2.

4. NUMERICAL SCHEME

The numerical investigation of the ideal gas passing the two-stage stator-rotor passage is based on an implicit finite-volume method. The fully compressible, 2D Navier-Stokes equations are solved for the physical domain. Turbulence is treated with a high Reynolds $k-\varepsilon$ model. A multidimensional second-order accuracy differencing scheme is used to calculate the density in order to improve the solution accuracy in the compressible flow. A third-order scheme is used to other parameters to discretise the finite-volume equations.

As the vane/blade number ratio is 1/1, the passage between two adjacent stator vanes and two adjacent rotor blades are included in the solution domain. A multiblock structured mesh is generated for each configuration. The grid topology is of HOH type. The computational grid as well as the enlarged leading and trailing edges are shown in Figure 2. It can be seen that the heads and the tails of the airfoils are described smoothly in the grid.

Total pressure, total temperature, and flow angle at the inlet, as well as the static pressure at the outlet, are defined according to the data listed in the Table 2.

5. RESULTS AND DISCUSSION

5.1. Entropy distribution

Entropy generation calculation is performed to obtain significant information that will improve our understanding of the physical phenomena involved in the turbomachinery. In the fixed and rotating blades system, the entropy-generation rate

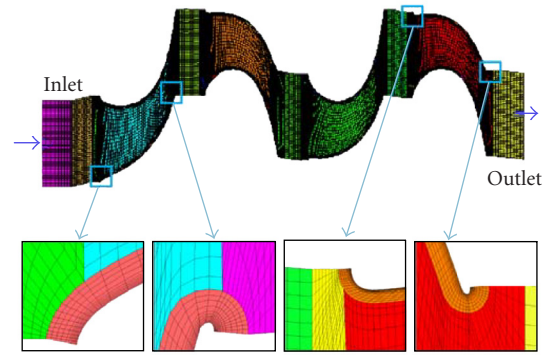

Figure 2: Computational grid.

comes from the blade boundary layer and the profile loss, as well as the wake region. Therefore, entropy distribution is able to imply the wake tracking in the passage.

Based on the resulted flow field, the entropy distribution in the passage is calculated locally by the following equation:

$$\Delta s = c_p \ln\left[\frac{T}{T_0}\right] - R\ln\left[\frac{p}{p_0}\right], \tag{1}$$

where s is the entropy, T is the temperature, p is the static pressure, while T_0 is the temperature 273.15 K and p_0 is the atmosphere pressure 1.013×10^5 Pa.

Steady calculation with the frozen rotor approach

Based on the frozen rotor approach, the entropy distributions at the clocking positions S1, S2, and S3 are shown in Figures 3a, 3b, and 3c, respectively. In each graph, the resulted entropy distributions at six stator-rotor positions are presented consequently. A pair of blades is grayed in order to show the different stator-rotor positions clearly.

Losses from wakes and boundary layers are obvious in the entropy distribution. Wakes are generated at the trailing edges of vanes and blades. They are represented by higher entropy than the surrounding flow field. Wake losses, boundary layer losses, and the profile losses make the entropy reach the maximum value at the outlet. Comparing the entropy distributions at the same stator-rotor relative position in Figures 3a, 3b, and 3c, it is obvious that the clocking causes the different entropy distributions. It implies that the different clocking positions will reach different turbine efficiency.

In each clocking position, not only wakes' directions, but also their magnitudes, vary continuously. Therefore, the different entropy distributions at the outlet are obtained at different stator-rotor positions.

Unsteady calculation with the sliding mesh approach

Based on the unsteady calculations, the entropy distributions at the clocking positions S1, S2, and S3 are shown in Figures 4a, 4b, and 4c, respectively.

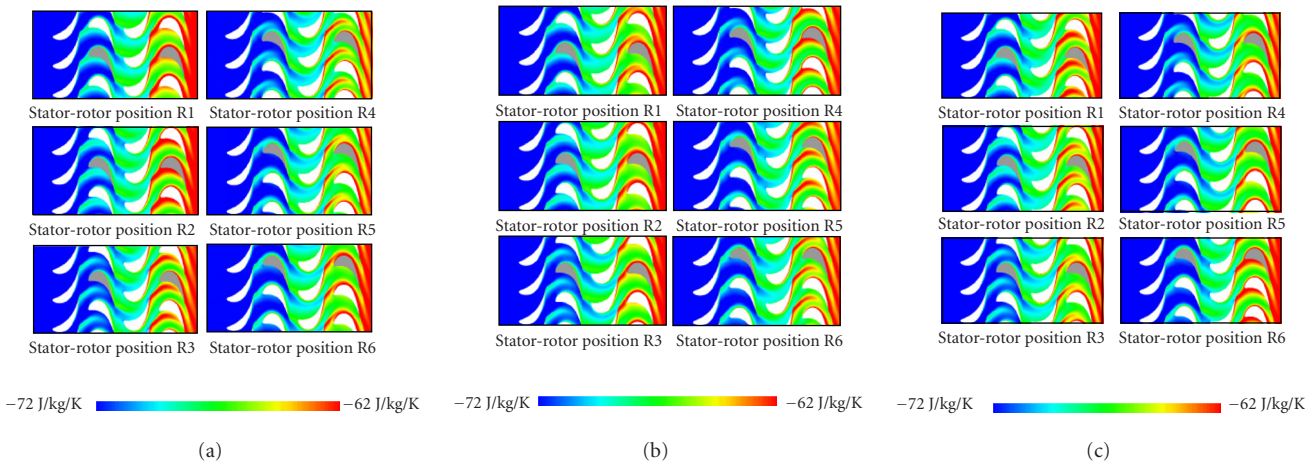

Figure 3: Entropy distributions in the steady calculations (frozen rotor approach): (a) clocking position S1, (b) clocking position S2, and (c) clocking position S3.

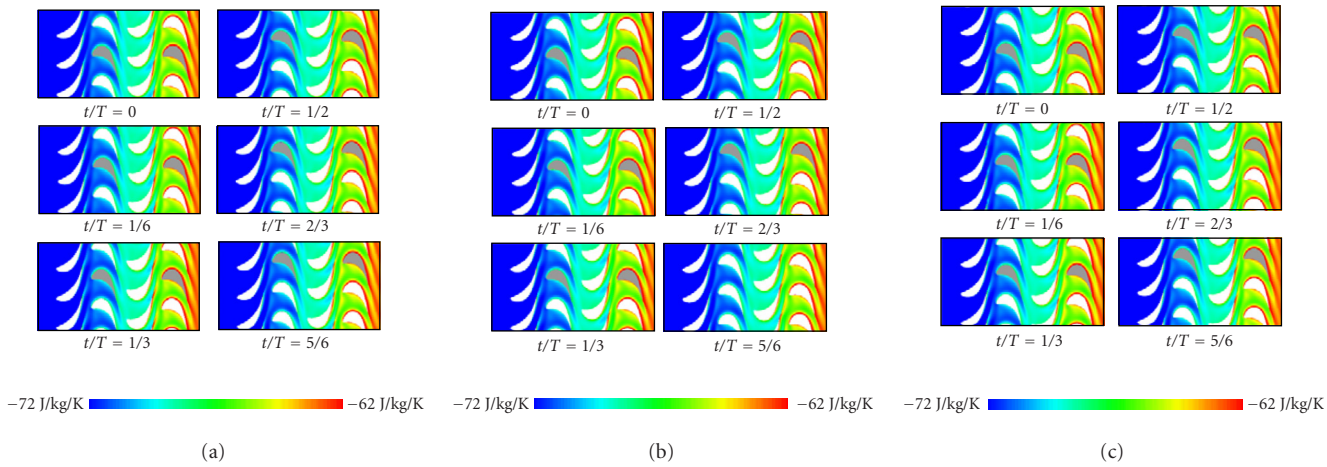

Figure 4: Entropy distributions in the unsteady calculation (sliding mesh approach): (a) clocking position s1, (b) clocking position s2, and (c) clocking position s3.

In each graph, the resulted entropy distributions at six chosen times are illustrated. The corresponding relationship between the six dimensionless times and the stator-rotor positions has been shown in the Table 1.

It is clear that the unsteadiness of the entropy is very strong in the turbine cascade. Wakes sweep one pitch of the next stator or rotor with different directions and magnitudes while the rotors move. It is similar to what is observed in the frozen rotor calculations. Comparing the entropy graphs at the same time in Figures 4a, 4b, and 4c, it is obvious that the clocking causes the different entropy distributions. It means that the different clocking positions will reach different efficiency, just like what have been concluded in the frozen rotor approach.

Comparing Figures 3 and 4, it is clear that the magnitude of the wakes resulted in the frozen rotor approach is significantly higher than that from the sliding mesh approach. It means the former approach generates artificial "wakes", originating from the interface between the rotor and the stator mesh. It implies that the loss of the flow field in the steady calculation is overestimated.

One notices also a distortion of the wake tracking in the Figure 3. The wakes from the unsteady calculation spread along the direction of the trailing edge of blades or vanes. But the wakes from the steady calculation start from the trailing edge of the blades or vanes and then blend down to the next stage. This is caused by that the interaction between the rotor and stator is not considered in the frozen rotor approach. As illustrated by the computation, the frozen rotor approach can calculate the wakes to some degree, but with some errors in magnitudes and directions. Therefore, it estimates the loss of the flow in an approximate way.

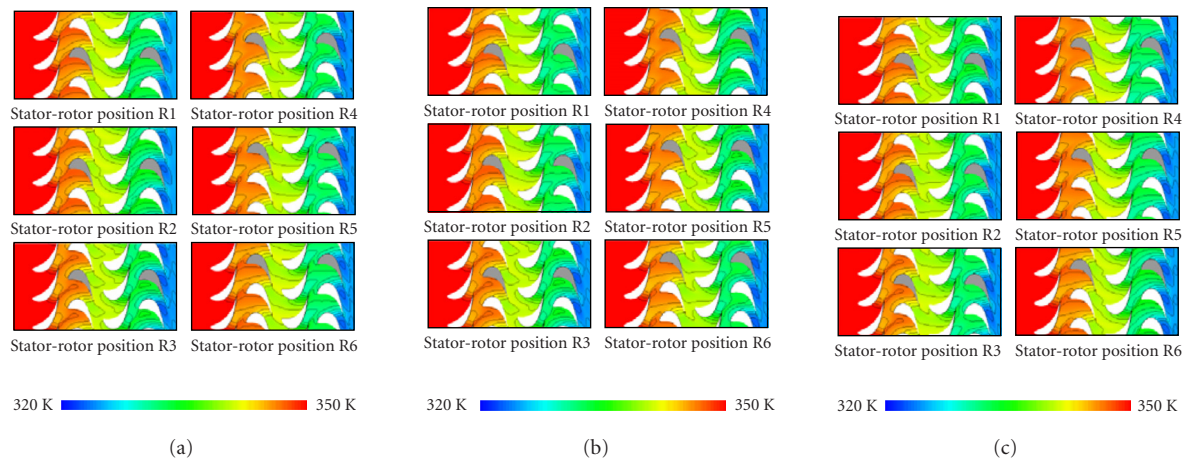

Figure 5: Absolute temperature distributions in the steady calculations (frozen rotor approach): (a) clocking position s1, (b) clocking position s2, and (c) clocking position S3.

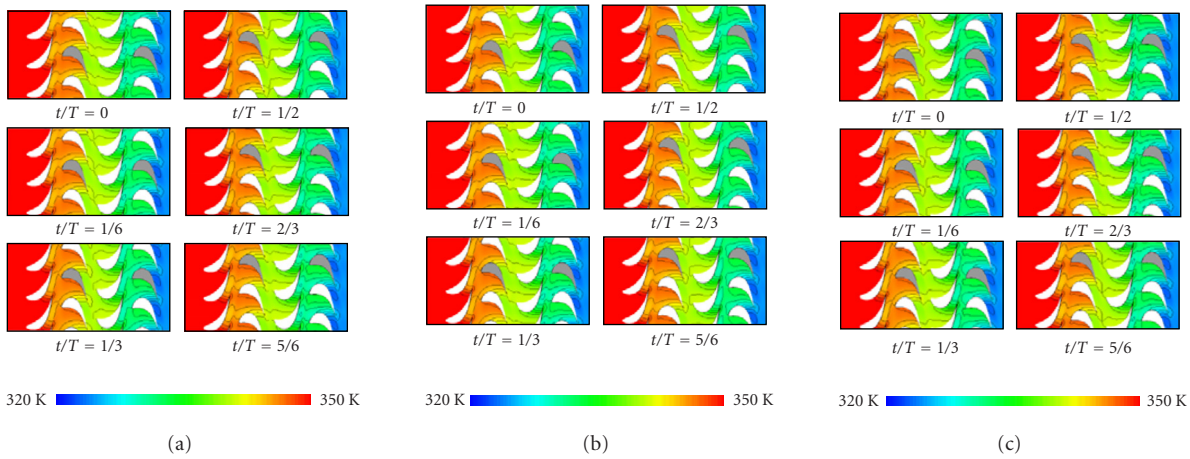

Figure 6: Absolute temperature distributions in the unsteady calculation (sliding mesh approach): (a) clocking position s1, (b) clocking position s2, and (c) clocking position s3.

5.2. Temperature distribution

Steady calculation with the frozen rotor approach

Based on the steady calculation with the frozen rotor approach, the temperature distributions are shown in Figures 5a, 5b, and 5c, for the three clocking positions S1, S2 and S3, respectively. Taking clocking position S1 as an example, it can be seen that the temperature varies continuously while the stator-rotor position. A different outlet temperature is reached at different stator-rotor position. This will influence the turbine efficiency obviously, as the outlet temperature is an important parameter in the efficiency calculation. At the clocking positions S2 and S3, the temperature distributions have a similar principle.

Comparing the correspondent graphs at the same stator-rotor positions, it can be seen that the temperature distributions in the first stage are almost the same at the three clocking positions. The influence of the clocking emphasizes the temperature distribution in the second stage as well as the outlet temperature.

Unsteady calculation with the sliding mesh approach

The temperature distributions at three clocking positions based on the unsteady calculation are shown in Figures 6a, 6b, and 6c, respectively.

Comparing the temperature distributions at the same dimensionless times t/T in the three clocking positions, the temperature distributions are almost the same in the first stage. The influence of the clocking on the temperature is mainly focused in the second stage, as it is observed in the results from the frozen rotor approach. But, the difference of the temperature at the outlet among the clocking positions is so small that it cannot even be distinguished from Figures 6a, 6b, and 6c.

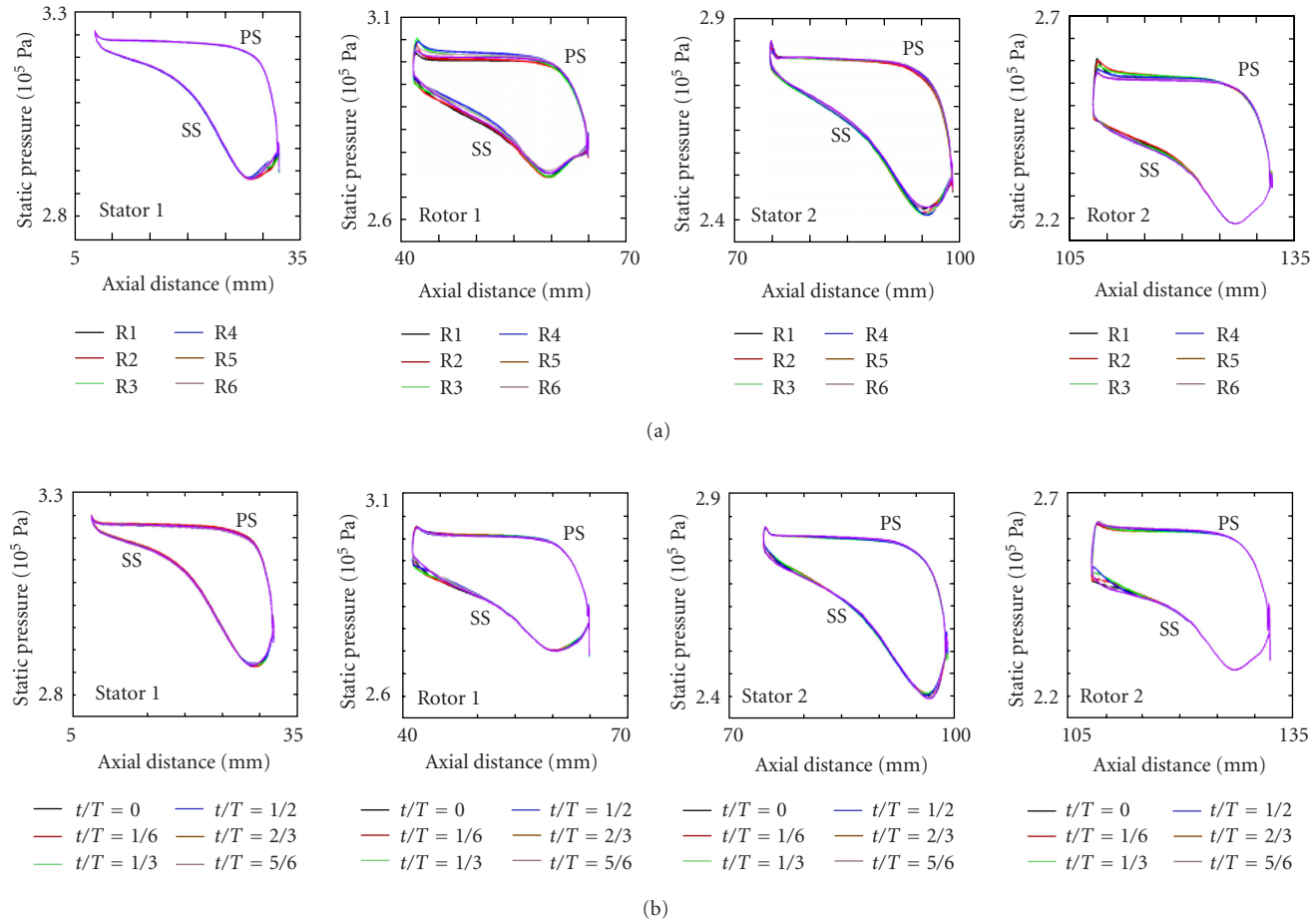

Figure 7: Static pressure distributions at clocking position S3. (a) Frozen rotor approach, steady calculation. (b) Sliding mesh approach, unsteady calculation.

The unsteady algorithm predicts the unsteadiness of the flow field while considering the rotor-stator interaction. Therefore, when the temperature distributions based on the frozen rotor approach are compared with those from the sliding mesh approach, it can be observed that the temperatures at the outlet in the unsteady algorithm are lower and more even than in the steady case.

5.3. Static pressure distribution

The static pressure distributions along the profiles at the clocking position S3 are shown in this section. Figures 7a and 7b illustrate the results based on the frozen rotor approach and the sliding mesh approach, respectively.

The static pressure along the vane of Stator 1 varies in an observable magnitude only at the trailing edge in both graphs. It means the different positions of Rotor 1 influence the upstream flow field and result in the different static pressure at the rear part of Stator 1. Stator 2 is influenced by both Rotor 1 and Rotor 2. Its static pressure varies along the whole profile at different stator-rotor positions. Both Rotor 1 and Rotor 2 have a significant pressure variation in the front part of the blades. As Rotor 1 has an interaction with Stator 2, the static pressure at the rear part of Rotor 1 varies too. The static pressure at the trailing edge of Rotor 2 keeps as a constant, which implies that the outlet pressure is steady during the rotation of the rotors.

Comparing Figures 6a and 6b, one notices that the static pressure distributions along the profiles are very similar to each other. More important is the static pressures at the leading edge of Stator 1 and the trailing edge of Rotor 2 are almost the same in the two approaches. It supports the idea of predicting the efficiency by the frozen rotor approach since the static pressures at the inlet and the outlet are two important parameters while calculating the total-to-total efficiency (see (2)).

Certainly, it is obvious that the static pressure variations in the results of the sliding mesh approach are weaker than those of the frozen rotor approach. Another difference between the two approaches occurs on the leading edge of the rotors. While the static pressure varies more significantly on the pressure side in the frozen rotor approach, it is stronger on the suction side in the sliding mesh approach. Both of

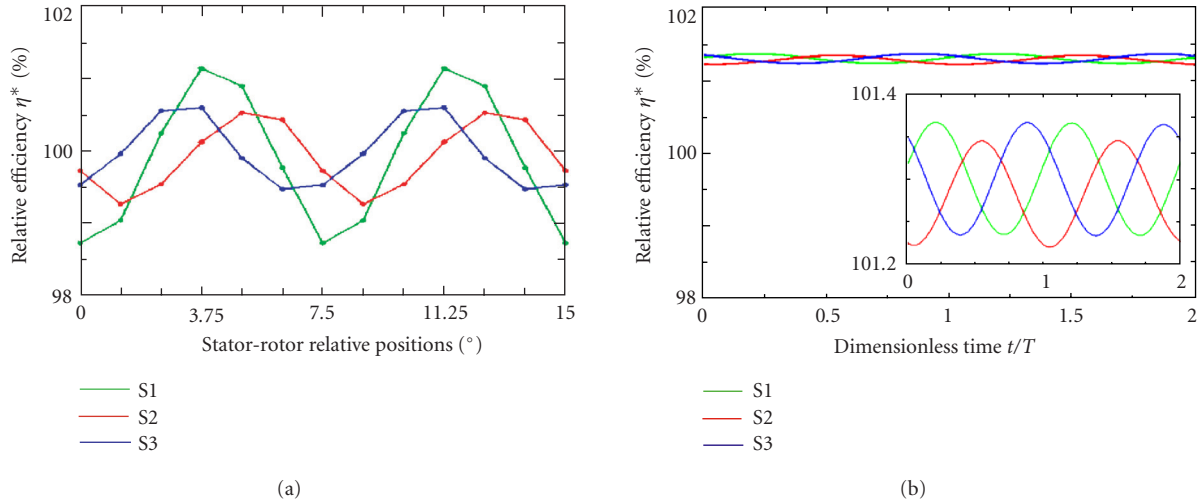

Figure 8: Relative efficiency distributions. (a) Frozen rotor approach, steady calculation. (b) Sliding mesh approach, unsteady calculation.

them are caused by different directions and magnitudes of wakes in two approaches, which have been discussed in the entropy distributions.

The averaged static pressure distributions at different clocking positions from both approaches have the similar principle, as what have been discussed above. It implies that estimating the clocking effect on the efficiency based on frozen rotor approach makes sense.

5.4. Efficiency estimation

In the presented investigation, the total-to-total efficiency is defined as

$$\eta = \frac{\gamma}{\gamma - 1} \frac{\ln\left(T_2/T_1\right)}{\ln\left(p_2/p_1\right)}, \tag{2}$$

where T_1 and T_2 are the mass-averaged temperature at the inlet and the outlet, p_1 and p_2 are the mass-averaged static pressure at the inlet and the outlet, γ is the specific heat ratio, and η is the efficiency.

The unsteady solution is time periodic while the stator-rotor position in the steady solution is spatial repeatable. Hence, in order to show the tendency more clearly, two periods of the total-to-total relative efficiency distributions based on the two approaches are presented in Figure 8. The relative efficiency is defined as

$$\eta^* = \frac{\eta}{\eta_0}, \tag{3}$$

where η_0 is the averaged total-to-total efficiency at the clocking position S1 based on the frozen rotor approach.

The amplitudes of the relative efficiency variation at different stator-rotor positions in Figure 8a are significantly larger than those in Figure 8b. As the static pressure at the inlet and the outlet from both approaches have no large difference, this error is mainly caused by the temperature difference at the outlet in each configuration.

In order to show the details of the relative efficiency distributions from the sliding mesh approach, an enlarged graph with a high resolution is put at the right bottom corner of Figure 8b. It can be observed that the curves in Figures 8a and 8b have similar tendency. They reach the peaks in the order of clocking positions S1, clocking positions S2, and clocking positions S3 from both approaches. If the curves are compared from the trigger position, it looks like the curves based on the frozen rotor approach are 2.5° forward than those based on the sliding mesh approach, although they have different amplitudes. The shift of the curves is possibly caused by the blending of the wakes in the frozen rotor approach. The efficiency curve at the clocking position S1 has the highest peak for both approaches, while the curve at the clocking position 2 has the lowest peak.

The averaged total-to-total relative efficiency η^*_{av} based on the frozen rotor approach is defined as the averaged value of the relative efficiency at the six stator-rotor positions in each clocking position. The averaged total-to-total relative efficiency η^*_{av} based on the unsteady results is calculated as the averaged value of the relative efficiency in one blade-passing period. This is shown in Table 3 and Figure 9.

The averaged relative efficiencies have the same tendency for both approaches: clocking position S3 has the highest averaged relative efficiency while the clocking position S2 has the lowest one. The estimated averaged relative efficiency from the frozen rotor approach is about 1.3% lower than that from the sliding mesh approach, which is mainly caused by the artificial "wakes" in the frozen rotor approach.

Clocking effects are evidenced by the averaged relative efficiency difference $\Delta\eta^*_{\text{av}}$, which is defined as

$$\Delta\eta^*_{\text{av}} = \eta^*_{\text{av}} - \left(\eta^*_{\text{av}}\right)_{\min}, \tag{4}$$

Table 3: Averaged relative efficiency distributions.

Clocking position	Averaged relative efficiency η^*_{av}(%) (frozen rotor approach)	Averaged relative efficiency η^*_{av}(%) (sliding mesh approach)
S1	100.00	101.29
S2	99.97	101.28
S3	100.03	101.31

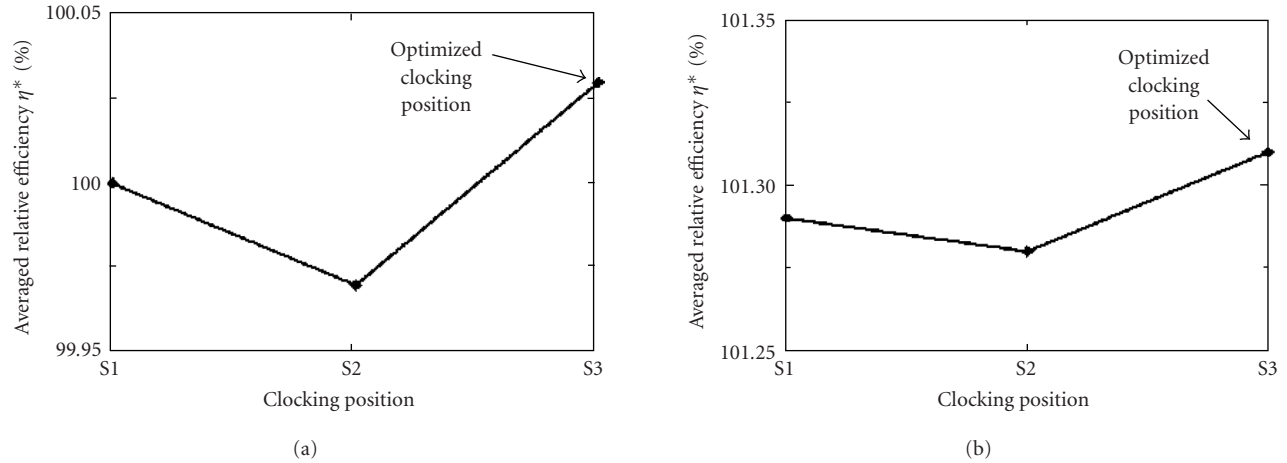

Figure 9: Averaged relative efficiency distributions. (a) Frozen rotor approach, steady calculation. (b) Sliding mesh approach, unsteady calculation.

where $(\eta^*_{av})_{min}$ is the minimum value of the averaged relative efficiency among the three clocking positions. It results from Table 3 that the maximum averaged relative efficiency difference based on the frozen rotor approach is 0.06% while it is 0.03% in the sliding mesh approach. The former is two times higher than the later. It means the frozen rotor approach enlarged the clocking effect on the turbine efficiency.

Based on the data contained in the Table 3 and Figure 9, both the frozen rotor approach and the sliding mesh approach predict that the clocking position S3 has the highest averaged relative efficiency, and therefore is the optimized clocking position. Hence, it is concluded that the frozen rotor approach has an ability to predict the clocking effect and the optimized clocking position qualitatively, although it can not estimate the turbine property as good as the unsteady calculation.

6. CONCLUSION

In the present paper, a frozen rotor approach in a steady calculation and a sliding mesh approach in an unsteady simulation are performed in a stator clocking investigation. Entropy, temperature, and pressure distributions in the flow fields from both approaches are presented and compared with each other. The efficiency variations as well as the optimized clocking positions are predicted based on the numerical results.

Both approaches result in the wakes generated at the trailing edge of blades or vanes. Their directions and magnitudes vary at different stator-rotor positions in a similar way. Since the interaction between the rotor and stator are not considered in the frozen rotor approach, the artificial "wakes" and the wake blending are obvious in their results.

The temperature distributions in the cascades and the static pressure distributions along the profiles from the two approaches follow the similar principles. One notices that the static pressures at the leading edge of Stator 1 as well as the trailing edge of the Rotor 2 are almost the same between the two approaches. But, the outlet temperature distributions in the unsteady calculation are obviously lower than those in the frozen rotor approach.

The relative efficiency distributions for two approaches show a similar tendency, although the results based on the frozen rotor approach have larger variation amplitudes. The averaged total-to-total relative efficiencies at three clocking positions have completely the same tendency from both approaches. The same optimized clocking positions are therefore predicted. The averaged relative efficiency difference resulted from the frozen rotor approach among the three clocking positions is two times higher than that from the sliding mesh approach. This means that frozen rotor approach enlarged the clocking effect on the turbine efficiency.

Overall, the frozen rotor approach has an ability to predict the clocking effect and the optimized clocking position

Table 4: Nomenclature.

Symbol	Unit of measurement	Notation
c_p	kJ / kg / K	Specific heat
PS	—	Pressure side
p	Pa	Pressure
S1, S2, S3	—	Clocking positions
SS	—	Suction side
s	kJ/kg/K	Entropy
T	K, s	Temperature, period
t	s	Time
Greek letters		
η	—	Total-to-total efficiency
γ	—	Specific heat ratio
Subscripts		
1	Inlet	
2	Outlet	
av	Averaged	
min	Minimum	
*	Relative	

qualitatively, although it omits some unsteady features in the turbines.

Certainly, some other elements can influence the clocking effect too in the two approaches, for example, 3D algorithm, turbulence model, and so on. More investigations focused on these elements will be done in the future.

ACKNOWLEDGMENTS

The investigation was performed as a part of the joint research program "500 MW auf einer Welle (AG Turbo)." The work was supported by the Bundesministerium für Wirtschaft (BMWI) under file number 0327061E. The authors gratefully acknowledge AG Turbo and ALSTOM Power, especially Dr. Michael Sell, for their support and permission to publish this paper. Thanks also to Mr. Christian Tümmers for the numerical calculations. The responsibility for the content lies with the authors.

REFERENCES

[1] F. Eulitz, K. Engel, and H. Gebing, "Numerical investigation of the clocking effects in a multistage turbine," in *ASME Turbo Expo 1996*, Birmingham, UK, June 1996, ASME paper 96-GT-26.

[2] U. Reinmöller, B. Stephan, S. Schmidt, and R. Niehuis, "Clocking effects in a 1.5 stage axial turbine—steady and unsteady experimental investigations supported by numerical simulations," in *ASME Turbo Expo 2001, International Gas Turbine & Aeroengine Congress & Exhibition*, New Orleans, La, USA, June 2001, ASME paper 2001-GT-0304.

[3] F. W. Huber, R. D. Johnson, O. P. Sharma, J. B. Staubach, and S. W. Gaddis, "Performance improvement through indexing of turbine airfoils: Part I—experimental investigation," *Journal of Turbomachinery*, vol. 118, pp. 630–635, 1996.

[4] L. W. Griffin, F. W. Huber, and O. P. Sharma, "Performance improvement through indexing of turbine airfoils: Part II—numerical simulation," *Journal of Turbomachinery*, vol. 118, pp. 636–642, 1996.

[5] A. Arnone, M. Marconcini, R. Pacciani, C. Schipani, and E. Spano, "Numerical investigation of airfoil clocking in a three-stage low pressure turbine," in *ASME Turbo Expo 2001, International Gas Turbine & Aeroengine Congress & Exhibition*, New Orleans, La, USA, June 2001, ASME paper 2001-GT-0303.

[6] D. J. Dorney, O. P. Sharma, and K. L. Gundy-Burlet, "Physics of airfoil clocking in a high-speed axial compressor," in *ASME Turbo Expo 1998*, Stockholm, Sweden, June 1998, ASME paper 98-GT-082.

[7] D. J. Dorney, R. R. Croft, D. L. Sondak, U. E. Stand, and C. Z. Twardochleb, "Computational study of clocking an embedded stage in a 4-stage industrial turbine," in *ASME Turbo Expo 2001, International Gas Turbine & Aeroengine Congress & Exhibition*, New Orleans, La, USA, June 2001, ASME paper 2001-GT-0509.

[8] P. Cizmas and D. Dorney, "Parallel computation of turbine blade clocking," AIAA-paper 98-3598, American Institute of Aeronautics and Astronautics, Reno, Nev, USA, 1998.

[9] D. Bohn, J. Ren, and M. Sell, "Influence of stator clocking on the unsteady three-dimensional flow in a two-stage turbine," *Journal of Turbomachinery*, vol. 127, no. 1, pp. 156–163, 2005.